Identification of surface oxygen vacancy-related phonon–plasmon coupling in TiO_2 single crystal*

Jun-Hong Guo(郭俊宏)[1], Ting-Hui Li(李廷会)[2], Fang-Ren Hu(胡芳仁)[1,†], and Li-Zhe Liu(刘力哲)[3,‡]

[1] *School of Optoelectronic Engineering and Grüenberg Research Center, Nanjing University of Posts and Telecommunicates, Nanjing* 210023, *China*

[2] *College of Electronic Engineering, Guangxi Normal University, Guilin* 541004, *China*

[3] *Nanjing National Laboratory of Microstructures and Department of Physics, Nanjing University, Nanjing* 210093, *China*

(Received 16 August 2016; revised manuscript received 29 August 2016; published online 25 October 2016)

Oxygen vacancies (OVs) play a critical role in the physical properties and applications of titanium dioxide nanostructures, which are widely used in electrochemistry and photo catalysis nowadays. In this work, OVs were artificially introduced in the surface of a pure TiO_2 single crystal by pulsed laser irradiation. Raman spectra showed that the intensity of E_g mode was enhanced. Theoretical calculations disclose that this was caused by the strong coupling effect between the phonon vibration and plasmon induced by the OVs-related surface deformation, and good agreement was achieved between the experiments and theory.

Keywords: luminescent materials, Raman scattering, oxygen vacancies

PACS: 71.20.Nr, 78.40.Fy, 78.30.–j **DOI:** 10.1088/1674-1056/25/12/127103

1. Introduction

Metal oxides have played important roles in scientific research and industrial production, because of their potential use in optical devices, catalysts, batteries, gas-sensors, and biosensors.[1–5] Among the different metal oxides, titanium dioxide (TiO_2) has attracted much attention due to its interesting applications such as water splitting, photo catalysis and gas sensing.[6–10] In various technological applications, nanosized materials have yielded excellent performance because of their small dimensions, i.e., the large surface-to-volume ratio. Nanoscale titanium dioxide such as nanotubes (NTs), nanocrystals (NCs), nanodisks, and nanowires have been fabricated and their optical and electronic characteristics and potential applications have been extensively studied.[11–14] Among these, many novel physical characteristics are simply ascribed to its oxygen vacancies, but cannot be confirmed with evidence.[15–18] Because the nanostructure is very complex, its intrinsic physical mechanism about OVs is still not clarified. Therefore, how to directly characterize and analyze the existing states of OV has become a crucial problem.

In order to clearly investigate the phonon characteristics of metal oxide nanomaterials with different OV types, we introduced OVs in the surface of a pure TiO_2 single crystal artificially by pulsed laser irradiation. Spectral analysis and theoretical calculations showed that strong coupling effect existed between the phonon relating to surface OVs and the plasmon induced by the surface deformation potential. This effect caused the intensity of Raman active mode E_g to increase while A_{1g} mode decreased. This work improves our understanding of the OVs properties in TiO_2 and is beneficial to further applications.

2. Experiment

A 248-mm laser beam with a 1-Hz repetition rate was selected to irradiate the TiO_2 single crystal (named sample A) via a 90° prism. The laser beam was a Gauss distribution of linear polarized light with the power of 451 mJ/pulse and the irradiation time was 5 s. A 20-times microscope objective was added to converge the laser to TiO_2 single crystal and also to enhance the laser intensity. After irradiation, the sample A was annealed in O_2 at 1000 °C for 5 h to prepare sample C. The Raman spectra of irradiated crystal (sample A), non-irradiated crystal (sample B), and the annealed crystal (sample C) were acquired on a T64000 triple Raman system at backscattering geometries using the 514.5-nm line of an Ar–ion laser as the excitation source. The diameter and power of the beam spot were 3 mm and 4.6 mW, respectively. The resolution of the spectrometer is 0.5 cm^{-1}. X-ray photoelectron spectroscopy (XPS) was performed on the PHI 5000 Versa Probe.

3. Results and discussion

Figure 1(a) provides the corrected XPS spectra of Ti 2p from samples A and B. It was clear to see the $2p_{3/2}$ peak at

*Project supported by the National Natural Science Foundation of China (Grant Nos. 61574080, 11404162, 61505085, and 61264008) and the Natural Science Foundation of Jiangsu Province, China (Grant No. BK20130549).

†Corresponding author. E-mail: hufr@njupt.edu.cn

‡Corresponding author. E-mail: lzliu@nju.edu.cn

© 2016 Chinese Physical Society and IOP Publishing Ltd

458.9 eV and $2p_{1/2}$ peak at 464.6 eV, and the Ti 2p peaks in all samples had only one component. Figure 1(b) is a larger image of the binding energies of Ti $2p_{3/2}$ in Fig. 1(a). The binding energy of sample A had a deviation of 0.2 eV compared to sample B, which resulted in the existence of OVs that changed the charge distribution around titanium atoms.[19] Based on the method introduced to calculate the OVs in SnO_2,[20,21] and according to the relationship between the binding energies of Ti $2p_{3/2}$ level versus the valences of Ti from pure TiO_{2-x}, the OV in sample A was 0.77%.

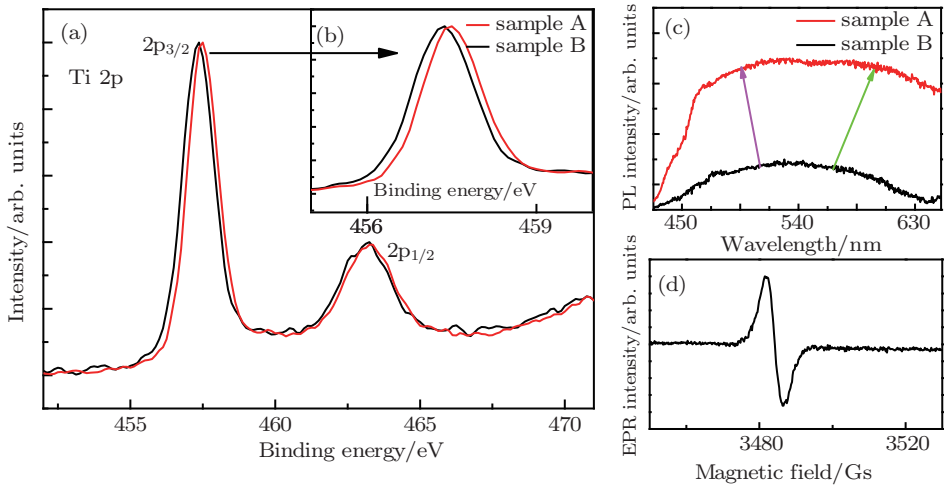


Fig. 1. (color online) (a) XPS spectra from samples A and B, and (b) larger image of the Ti $2p_{3/2}$ spectra, (c) PL spectra from samples A and B, (d) EPR spectra of sample A. The unit 1 Gs = 10^{-4} T.

To clarify the existence of OVs, PL spectra were acquired from the two samples and shown in Fig. 1(c). The PL features composed of a double-peak structure could be observed and the energy separation between two subpeaks increases after irradiation. Since a large number of OVs will exist after irradiation, both the adsorbed oxygen atoms and OVs on the surface of crystals may be responsible for the double-peak PL. The difference in the applied stress caused by OVs on the inner and outer surfaces of crystals increases and it causes the increased splitting and shifting of the PL peak. To further investigate OVs existed on the surface of crystals, the EPR was shown in Fig. 1(d). The Landeg value was obtained to be 2.002 which has good consistency with previous reports.[22] The above experiments further confirmed the existence of OVs on the surface of TiO_2 crystals. However, the type of OVs in sample A was still not clear. In order to investigate the type of OVs produced by irradiation, Raman spectra were acquired from samples A and B and the corresponding results were shown in Fig. 2(a). The peaks at 235, 449, 611 cm^{-1} correspond to the well-known multi-phonon process, E_g and A_{1g} optical modes of the TiO_2 crystals.[23] However, the intensity of E_g mode had enhanced after irradiation. In addition, the Raman spectrum of annealed sample A was also shown in Fig. 2(a). Comparing the Raman spectra of sample, A and the annealing sample A, the intensity of E_g mode decreased obviously after annealing. To further investigate the intensity changes of vibration modes, we examined the temperature-dependent Raman spectra of the irradiated sample (sample A) and the results were displayed in Fig. 2(b). With decreasing measurement temperature from 300 K to 77 K, the location and peak shape of the Raman mode were relatively unchanged, but the intensity underwent an obvious increase. However, it is generally assumed that the effects of thermal expansion and a harmonic coupling to other phonons during the temperature increasing can cause the intensity reduction and simultaneous red-shift

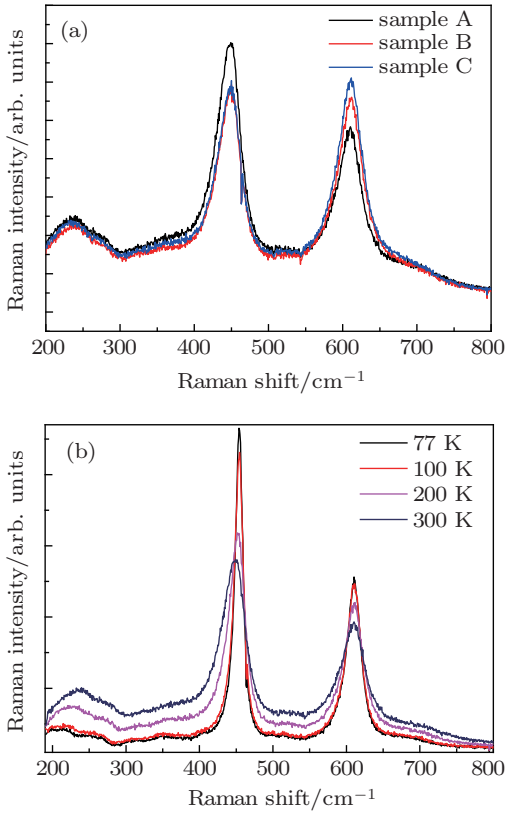


Fig. 2. (color online) (a) Raman spectra of samples A and B at room temperature and Raman spectra of annealed sample A, (b) temperature-dependent Raman spectra of sample A.

of the Raman spectra,[24,25] which is obviously contrary to our results. So this anomalous behavior needs to be clarified.

Density functional theory (DFT) calculations were conducted to theoretically confirm the anomalous behavior of Raman spectra. The optimized primitive TiO_2 with $a = 4.59$ Å, $b = 2.96$ Å lattice constant was shown in Figs. 3(a) and 3(b). The optimized structure lead to two typical Raman modes E_g (449 cm^{-1}) and A_{1g} (611 cm^{-1}), as shown in Figs. 3(c) and 3(d), respectively. We can infer that those Raman modes with different vibration direction can exhibit different Raman features, which also strongly depended on its surficial structure deformation.

Our calculations were performed under the framework of DFT as implemented in the CASTEP package. Electron–ion interactions were described by the projector augmented plane wave method, and the wave function was expanded in a plane wave basis set with an energy cutoff of 500 eV. The k points in the Brillouin zone were sampled on a $5\times5\times8$ mesh. The norm-conserving pseudo-potential method was chosen together with the gradient correction and the Perdew–Burke–Ernzerhof potential function.[26] Finally, the optimized geometrical structure was employed for construction and the diagonalized Hessian matrix:

$$D^{k,k'}_{\alpha,\alpha'} = \frac{1}{\sqrt{M_k M_{k'}}} \sum_{\alpha} \psi^{k,k'}_{\alpha,\alpha'} \, \mathrm{e}^{-\mathrm{i}\boldsymbol{q}\cdot\boldsymbol{r}_\alpha}, \tag{1}$$

where $\psi^{k,k'}_{\alpha,\alpha'}$ were the matrix force constants related to bond length and bond angle. The vibrational frequencies were obtained as the square roots of the phonon wave-vector $\boldsymbol{q} = 0$. The ratio of atom mass and bond length of Ti and O atoms were respectively. The optimized cell eigenfrequency can be simply written as:[27]

$$\omega_0^2 = 1/m_{\mathrm{Ti(O)}} \sum_{i=1}^{n} k_{\mathrm{Ti(O)}} \tag{2}$$

where $m_{\mathrm{Ti(O)}}$ was Ti(O) atom mass and $k_{\mathrm{Ti(O)}}$ is the corresponding parameters determined by Ti–O bond length and force constants. From the vibration of E_g and A_{1g} modes in Figs. 3(c)–3(d), we can see that its Raman mode behavior strongly depended on their symmetrical structure change. The TiO_2 structures were characterized by two different types along (001) direction, as shown in Fig. 3(b).

In Fig. 4(a), we showed the calculated Raman spectra of TiO_2 at different temperature. According to the calculated Raman spectra, the intensity of the E_g and A_{1g} modes both increased when temperature decreased. But the intensity changes of both modes were basically the same, which was quite different from the experiment results shown in Fig. 2(b).

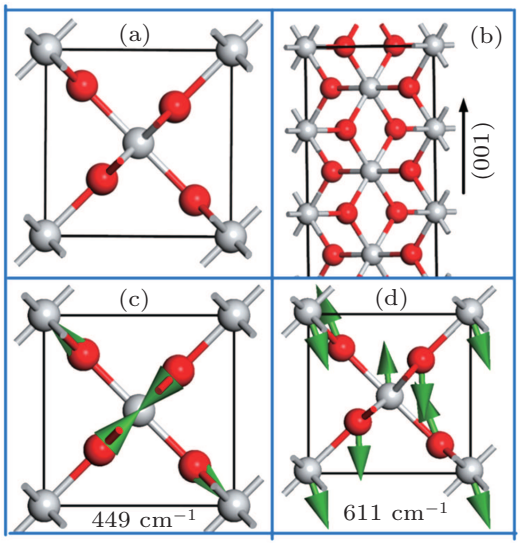


Fig. 3. (color online) (a) Optimized structure of TiO_2 cell used in the DFT calculations, (b) optimized structure of TiO_2 along the direction of (001), (c) vibration of E_g Raman mode, and (d) vibration of A_{1g} Raman mode.

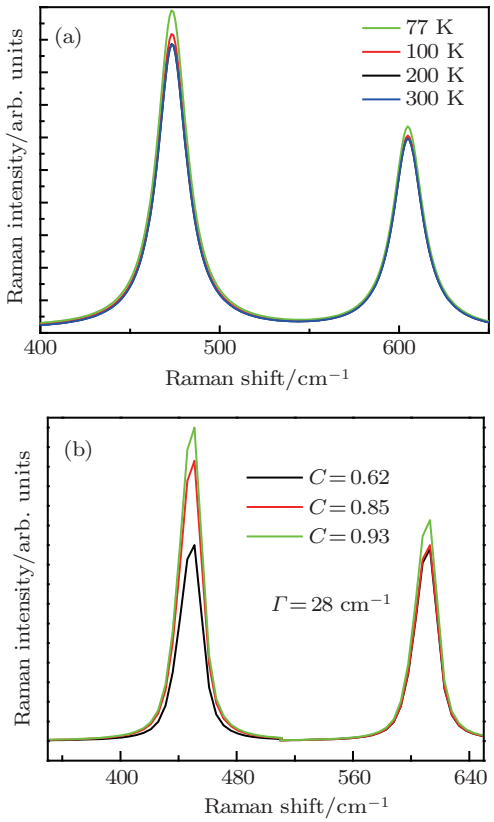


Fig. 4. (color online) (a) The Raman spectra of TiO_2 surface calculated by DFT, (b) the Raman spectra of TiO_2 surface calculated by phonon–plasmon coupling mechanism.

By considering the deformation potential in the surface layer caused by the phonon–plasmon coupling mechanism, the Raman spectrum could be calculated by[28]

$$I(\omega) = \frac{\mathrm{d}^2 S}{\mathrm{d}\omega \mathrm{d}\Omega} \propto \mathrm{Im}\left(-\frac{A(\omega)}{\varepsilon(\omega)}\right), \tag{3}$$

$$A(\omega) = C^2 B^2 \chi_{\mathrm{ph}}(\varepsilon_\infty + 4\pi\chi_{\mathrm{fc}}) - 2CB\varepsilon_\infty\chi_{\mathrm{ph}} - \frac{\varepsilon_\infty^2}{4\pi}, \tag{4}$$

where the Faust–Henry coefficient C_{FH} had been modified into

$$C = C_{\mathrm{FH}} \left\{ \frac{\varepsilon(r)_{\infty \mathrm{m}} \omega_{\mathrm{T}}^2 [\omega(r)_{\mathrm{Tm}}^2]}{f_{\infty} \omega_{\mathrm{Tm}}^2 (\omega_{\mathrm{A}}^2 - \omega_{\mathrm{E}}^2)} \right\}^{1/2}, \tag{5}$$

which depends on the E_{g} and $A_{1\mathrm{g}}$ mode frequencies ω_{E} and ω_{A} and the high-frequency dielectric constant $\varepsilon_{\infty m}$ of the surface layer $B = \omega_{\mathrm{E}}^2/(\omega_{\mathrm{A}}^2 - \omega_{\mathrm{E}}^2)$, and the total dielectric function $\varepsilon(\omega)$ was considered to be due to contributions from phonons and plasmons:

$$\varepsilon(\omega) = \varepsilon_{\infty} \left(1 + \frac{\omega_{\mathrm{A}}^2 - \omega_{\mathrm{E}}^2}{\omega_{\mathrm{E}}^2 - \omega^2 - \mathrm{i}\omega\Gamma} - \frac{\omega_{\mathrm{P}}^2}{\omega(\omega + \mathrm{i}\gamma)} \right). \tag{6}$$

Here ω_{p} was the plasma frequency, χ_{ph} was the free-carrier susceptibility, χ_{fc} was the ionic susceptibility, and $\Gamma$and γ were the phonon and plasmon damping constants, respectively. In the calculation, $\omega_{\mathrm{E}} = 449$ cm^{-1}, $\omega_{\mathrm{A}} = 611$ cm^{-1}, $\varepsilon_{\infty} = 7.95$, $\omega_{\mathrm{p}} = 17.5$ cm^{-1}, and $\gamma = 60$ cm^{-1}.[29] $\Gamma = 28$ cm^{-1} and C = 0.93 were adjustable parameters related to the deformation potential induced by the lattice imperfection near the surface and carrier changes. After considering the coupled phonon–plasmon effect, the measured Raman spectra of irradiated TiO_2 can be fitted well, as shown in Fig. 4(b). Those experimental and theoretical results implied that the superficial plasmon induced by OVs played an important role in its Raman behaviors.

4. Conclusions

In conclusion, we have revealed that when OVs are introduced in the surface of TiO_2, the phonon vibration of OVs and the plasmon induced by the surface deformation potential must be considered together. This leads to the large enhancement of the E_{g} mode intensity.

Acknowledgments

The calculation was carried out at the High Performance Computing Center of Nanjing University.

References

[1] Reddy B M and Khan A 2005 *Catal. Rev. Sci. Eng.* **47** 257
[2] Idota Y, Kubota T, Matsufuji A, Maekawa Y and Miyasaka T 1997 *Science* **276** 1395
[3] Brovelli S, Chiodini A, Lauria A, Meinardi F and Paleari A 2006 *Phys. Rev. B* **73** 073406
[4] Kucheyev S O, Baumann T F, Sterne P A, Wang Y M, Buuren T, Hamza A V, Terminello L J and Willey T M 2005 *Phys. Rev. B* **72** 035404
[5] Fröschl T, Hörmann U, Kubiak P, Kučerová G, Pfanzelt M, Weiss C K, Behm R J, Hüsing N, Kaiser U, Landfesterd K and Wohlfahrt-Mehrens M 2012 *Chem. Soc. Rev.* **41** 5313
[6] Sumita M, Hu C P and Tateyama Y 2010 *J. Phys. Chem. C* **114** 18529
[7] Kato H, Asakura K and Kudo A 2003 *J. Am. Chem. Soc.* **125** 3082
[8] Fujishima A, Rao T N and Tryk D A 2000 *J. Photochem. Photobiol. C* **1** 1
[9] Zeng W, Liu T, Wang Z C, Tsukimoto S S, Saito M and Ikuhara Y 2010 *Mater. Trans.* **51** 171
[10] Linsebigler A L, Lu G Q and Yates J T 1995 *Chem. Rev.* **95** 735
[11] Jeon K S, Oh S D, Sun Y D, Yoshikawa H Y, Masuhara H and Yoon M 2009 *Phys. Chem. Chem. Phys.* **11** 534
[12] Bavykin D V, Gordeev S N, Moskalenko A V, Lapkin A A and Walsh F C 2008 *J. Phys. Chem. B* **109** 8565
[13] Wu J M, Shih H C and Wu W T 2006 *Nanotechnology* **17** 105
[14] Abazović N D, Čomor M I, Dramicánin M D, Jovanović D J, Ahrenkiel S P and Nedeljković J M 2006 *J. Phys. Chem. B* **110** 25366
[15] Wang D Z, Wen S L, Chen J, Zhang S Y and Li FQ 1994 *Phys. Rev. B* **49** 14282
[16] Maki-Jaskari M A and Rantala T T 2002 *Phys. Rev. B* **65** 245428
[17] Verma R, Mantri B, Ramphal and Srivastava A K 2015 *Adv. Mater. Lett.* **6** 324
[18] Zhao Z H, Tian J, Sang Y, Cabot A and Liu H 2015 *Adv. Mater.* **27** 2557
[19] Liu L Z, Wu X L, Li T H and Shen J C 2015 *Appl. Surf. Sci.* **347** 265
[20] Wang D N, Miller A C and Notis M R 1996 *Surf. Interface Anal.* **24** 127
[21] Liang C H, Shimizu Y, Sasaki T and Koshizaki N 2003 *J. Phys. Chem. B* **107** 9220
[22] Li Y Z, Hwang D S, Lee N H and Kim S J 2005 *Chem. Phys. Lett.* **404** 25
[23] Arsov L D, Kormann C and Plieth W 1991 *J. Raman Spectra* **22** 573
[24] Samanta K, Bhattacharya P and Katiyar R S 2007 *Phys. Rev. B* **75** 035208
[25] Wu X L, Xiong S J, Sun L T, Shen J C and Chu P K 2009 *Small* **5** 2823
[26] Liu L Z, Li T H, Wu X L, Shen J C and Chu P K 2012 *J. Raman Spectra* **43** 1423
[27] Liu L Z, Wu X L, Shen J C, Li T H, Gao F and Chu P K 2010 *Chem. Commun.* **46** 5539
[28] Katayama S and Murase K 1977 *J. Phys. Soc. Jpn.* **42** 886
[29] Mitev P D, Hermansson K, Montanari B and Refson K 2010 *Phys. Rev. B* **81** 134303